

Electronic Supplementary Information (ESI)

Novel Molecular Triad Exhibiting Aggregation-Induced Emission and Thermally Activated Fluorescence for Efficient Non-doped Organic Light-Emitting Diodes

Hyung Jong Kim,^a Seong Keun Kim,^b Mallesham Godumala,^a Jiwon Yoon,^a Chae Yeong Kim,^a Ji-Eun Jeong,^a Han Young Woo,^a Jang Hyuk Kwon,^b Min Ju Cho*^a and Dong Hoon Choi*^a

^a Department of Chemistry, Research Institute for Natural Sciences, Korea University, 145 Anam-ro, Seongbuk-gu, Seoul, 02841, Republic of Korea

^b Department of Information Display, Kyung Hee University, 26 Kyungheedaero, Dongdaemun-gu, Seoul, 02447, Republic of Korea

E-mail: chominju@korea.ac.kr, dhchoi8803@korea.ac.kr

Table of Contents

1. Instrumentation, Materials, and Synthesis	S1
2. DFT Calculation Results in Optimized Geometries	S5
3. Photophysical, Electrochemical, and Thermal Properties	S6
4. TADF-OLED Device Fabrication and Characterization	S12
5. Additional Information	S18
6. References	S19

1. Instrumentation, Materials, and Synthesis

1-1. Instrumentation

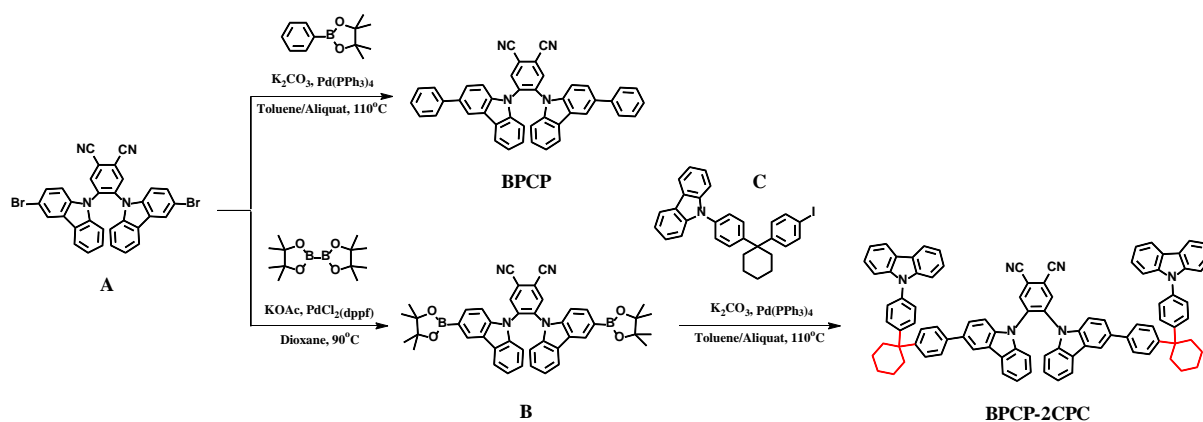
^1H and ^{13}C nuclear magnetic resonance spectra were recorded in deuterated chloroform on a Bruker 500 MHz spectrometer. A Thermo Scientific Flash 2000 (Thermo Fisher Scientific) elemental analyzer was used to identify the content of C, H, N, S, and O. Matrix-assisted laser desorption ionization time-of-flight mass spectrometry (MALDI-TOF/TOFTM 5800 system (AB SCIEX)) was used to determine the mass of the compounds; the experiments were performed at the Korea Basic Science Institute (Seoul).

The absorption spectra in the solution and film states were obtained using a UV-vis absorption spectrophotometer (Agilent 8453, photodiode array, $\lambda = 190\text{--}1100$ nm). The film samples were fabricated on cleaned glass substrates by the spin-coating method using 1.0 wt% toluene solutions. Photoluminescence (PL) spectra of the solution and film states were recorded using a Hitachi F-7000 fluorescence spectrophotometer. Transient PL spectra were acquired when the photon count reached 10000, under nitrogen atmosphere, using a Quantaaurus-Tau fluorescence lifetime measurement system (C11367-03, Hamamatsu Photonics Co.). Differential scanning calorimetry (DSC, Mettler STAR^e) was used to identify the thermal properties at a heating ratio of $10\text{ }^\circ\text{C min}^{-1}$ under nitrogen atmosphere. Thermogravimetric analysis (TGA, Mettler STAR^e) was performed at a heating rate of $10\text{ }^\circ\text{C min}^{-1}$ under nitrogen atmosphere. The electrochemical properties of the host and emitting materials were measured by cyclic voltammetry (CV) using a potentiostat (eDAQ, EA161). Tetrabutylammonium hexafluorophosphate (0.10 M; Bu_4NPF_6) in distilled acetonitrile was used as the electrolyte solution, and Ag/AgCl and platinum wire (diameter: 0.5 mm) were used as the reference and counter electrodes, respectively. Thin films were prepared on a Pt plate using the drop-casting method. The absolute PL quantum yields (PLQYs) were determined by using a JASCO (FP-8600) spectrofluorometer with a xenon lamp excitation source, using an integrating sphere (ILF-835) for the solution and film samples.

1-2. Materials

In this study, all commercial reagents and solvents for synthesis of the host and emitting materials were purchased from Thermo Fisher Scientific Chemicals, Sigma-Aldrich, and Tokyo Chemical Industry (TCI). 9,9'-(Cyclohexane-1,1-diylbis(4,1-phenylene))bis(9H-carbazole) (**C-2PC**),¹⁻² 4,5-bis(3-bromo-9H-carbazol-9-yl)phthalonitrile (**A**),³ and 9-(4-(1-(4-iodophenyl)cyclohexyl)phenyl)-9H-carbazole (**C**)⁴ were prepared by following methods previously reported in the literature.

1-3. Synthesis



Scheme S1 Synthesis route for **BPCP** and **BPCP-2CPC**.

(1) 4,5-Bis(3-(4,4,5,5-tetramethyl-1,3,2-dioxaborolan-2-yl)-9H-carbazol-9-yl)phthalonitrile (**B**)

4,5-Bis(3-bromo-9H-carbazol-9-yl)phthalonitrile (**A**) (800 mg, 1.3 mmol) was added to 1,4-dioxane (30 ml) in a 100 ml two-neck round-bottom flask. Bis(pinacolato)diboron (990 mg, 3.9 mmol) and potassium acetate (760 mg, 7.8 mmol) were added to the reaction mixture, and [1,1'-bis(diphenylphosphino)ferrocene]dichloropalladium(II) (73 mg, 0.1 mmol) was then added to the mixture, which was then kept at $90^\circ C$ for 18 h under nitrogen. After cooling to room temperature, the solution was concentrated under reduced pressure. The residue was collected by filtration and purified by silica-gel column chromatography (eluent: ethyl acetate/hexane = 1:3, v/v) to obtain the required compound (**B**) as a yellow product in 60% yield. 1H NMR (500 MHz, $CDCl_3$): δ (ppm) 8.32 (s, 2H), 8.30 (d, $J = 1.85$ Hz, 2H), 7.86 (t, $J = 7.35$ Hz, 2H), 7.57 (t, $J = 7.35$ Hz, 2H), 7.02–7.16 (m, 8H), 1.32–1.38 (m, 24H). ^{13}C NMR (125 MHz, $CDCl_3$): 140.54, 138.42, 135.53, 132.96, 127.78, 126.35,

124.50, 124.00, 122.09, 121.76, 120.75, 114.93, 109.10, 108.41, 83.87, 25.02, 24.84. Anal. Calcd. for C₄₄H₄₀B₂N₄O₄: C, 74.39; H, 5.68; B, 3.04; N, 7.88; O, 9.01. Found: C, 74.21; H, 5.49; B, 3.15; N, 8.01; O, 9.14.

(2) 4,5-Bis(3-phenyl-9H-carbazol-9-yl)phthalonitrile (BPCP)

4,5-Bis(3-bromo-9H-carbazol-9-yl)phthalonitrile (**A**) (550 mg, 0.89 mmol) and phenyl boronic acid (420 mg, 2.05 mmol) were dissolved in anhydrous toluene (30 ml) in a 100 ml two-neck round-bottom flask. A few drops of Aliquat 336 (as a surfactant) and 2 M potassium carbonate (2 ml) were added to the reaction mixture, which was then degassed with nitrogen. Tetrakis(triphenylphosphine)palladium(0) (52 mg, 0.04 mmol) was added to the reaction mixture, which was then kept at 110 °C for 18 h under nitrogen. After cooling to room temperature, the solution was concentrated under reduced pressure. The residue was collected by filtration and purified by silica-gel column chromatography (eluent: dichloromethane/hexane = 3:1, v/v) to obtain the required compound (**BPCP**) as a yellow product in 74% yield. ¹H NMR (500 MHz, CDCl₃): δ(ppm) 8.36 (s, 2H), 8.03 (d, *J* = 9.75 Hz, 2H), 7.85–7.90 (m, 2H), 7.56 (t, *J* = 6.4 Hz, 4H), 7.43 (t, *J* = 7.35 Hz, 4H), 7.29–7.37 (m, 5H), 7.15–7.20 (m, 5H), 7.10–7.13 (m, 2H). ¹³C NMR (125 MHz, CDCl₃): 141.05, 141.03, 138.85, 138.81, 138.45, 137.83, 137.76, 135.48, 135.11, 128.82, 127.16, 126.98, 1226.56, 126.46, 125.64, 125.56, 124.96, 124.53, 124.48, 121.93, 121.88, 120.60, 120.57, 118.90, 114.81, 114.50, 109.35, 109.20, 109.13. Anal. Calcd. for C₄₄H₂₆N₄: C, 86.53; H, 4.29; N, 9.17. Found: C, 86.10; H, 4.71; N, 9.20. Mass *m/z* [(M + H)⁺] calcd for 610.22, found 610.14.

(3) 4,5-Bis(3-(4-(1-(4-(9H-carbazol-9-yl)phenyl)cyclohexyl)phenyl)-9H-carbazol-9-yl)phthalonitrile (BPCP-2CPC)

4,5-Bis(3-(4,4,5,5-tetramethyl-1,3,2-dioxaborolan-2-yl)-9H-carbazol-9-yl)phthalonitrile (**B**) (500 mg, 0.7 mmol) and 9-(4-(1-(4-iodophenyl)cyclohexyl)phenyl)-9H-carbazole (**C**) (740 mg, 1.41 mmol) were dissolved in anhydrous toluene (30 ml) in a 100 ml two-neck round-bottom flask. A few drops of Aliquat 336 (as a surfactant) and 2 M potassium carbonate (2 ml) were added to the reaction

mixture, which was then degassed with nitrogen. Tetrakis(triphenylphosphine)palladium(0) (41 mg, 0.03 mmol) was added to the reaction mixture, which was then kept at 110 °C for 18 h under nitrogen. After cooling to room temperature, the solution was concentrated under reduced pressure. The residue was collected by filtration and purified by silica-gel column chromatography (eluent: dichloromethane/hexane = 2:1, v/v) to obtain the required compound (**BPCP-2CPC**) as a yellow product in 68% yield. ¹H NMR (500 MHz, CDCl₃): δ(ppm) 8.36 (s, 2H), 8.10–15 (m, 4H), 8.00–8.05 (m, 2H), 7.84–7.87 (m, 2H), 7.35–7.57 (m, 26H), 7.23–7.33 (m, 5H), 7.13–7.18 (m, 5H), 7.08–7.12 (m, 2H). ¹³C NMR (125 MHz, CDCl₃): 140.88, 138.80, 138.37, 138.19, 135.44, 134.96, 134.66, 128.44, 127.78, 127.06, 126.69, 126.45, 125.81, 125.50, 124.85, 123.30, 121.87, 120.58, 120.27, 119.80, 118.73, 114.75, 114.51, 109.92, 109.33, 109.12, 46.07, 37.21, 26.38, 22.98. Anal. Calcd. for C₉₂H₆₈N₆: C, 87.87; H, 5.45; N, 6.68. Found: C, 88.44; H, 5.55; N, 6.01. Mass *m/z* [(M + H)⁺] calcd for 1256.55, found 1257.36.

2. Optimized Geometries from DFT Calculation

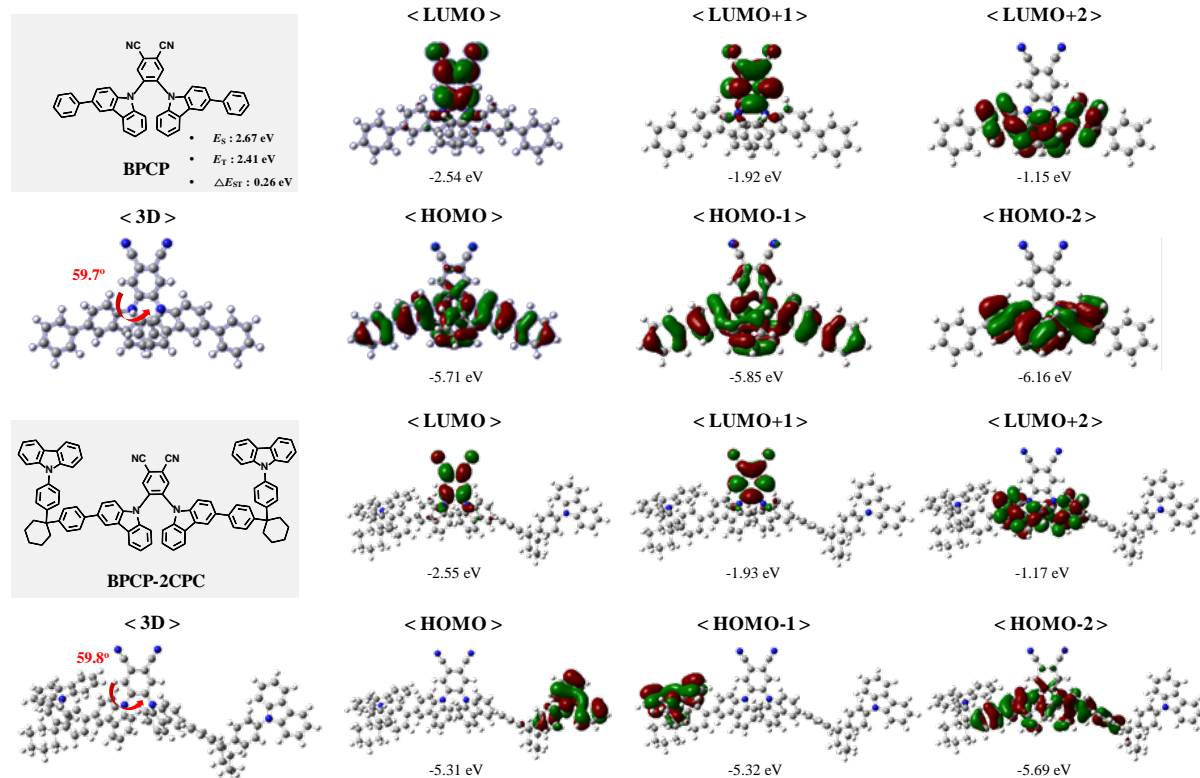


Fig. S1 Optimized geometries and calculated HOMO and LUMO spatial distribution for **BPCP** and **BPCP-2CPC**.

Density functional theory (DFT) calculations were performed at the B3LYP/6-31G* level of theory to determine the highest occupied molecular orbital (HOMO) and the lowest unoccupied molecular orbital (LUMO) distribution, and the excited state energies (E_S and E_T) of the designed molecules (Fig. S1). The computed ΔE_{ST} value of **BPCP** was found to be small due to the well-separated HOMO and LUMO distributions, indicating that **BPCP** is a potentially TADF-active material. Thus, **BPCP-2CPC**, in which the two host moieties are linked to **BPCP** through a non-conjugated linker, is also expected to exhibit TADF characteristics.

3. Photophysical, Electrochemical, and Thermal Properties

3-1. Solvatochromic Behavior of BPCP and BPCP-2CPC

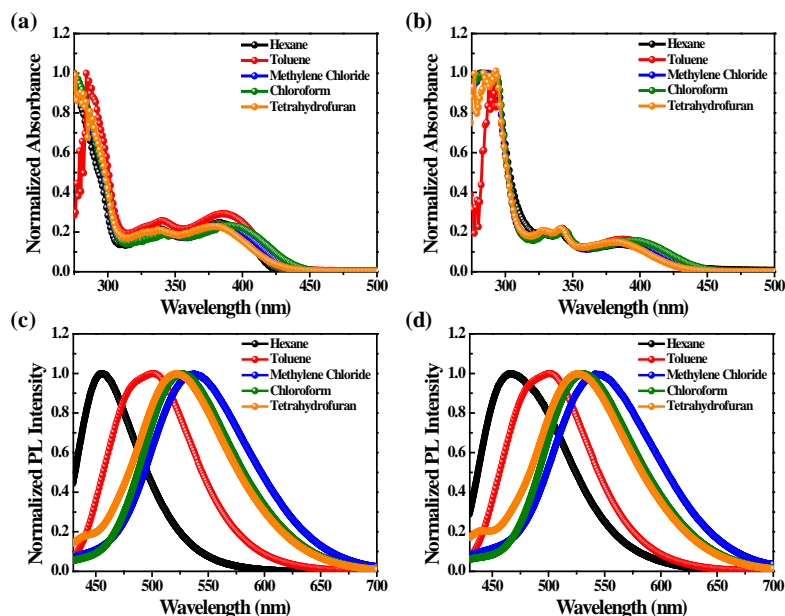


Fig. S2 UV-vis spectra and normalized photoluminescence (PL) spectra of (a,c) BPCP and (b,d) BPCP-2CPC in solvents with different polarities.

3-2. PL spectral behavior with the concentration of BPCP and BPCP-2CPC

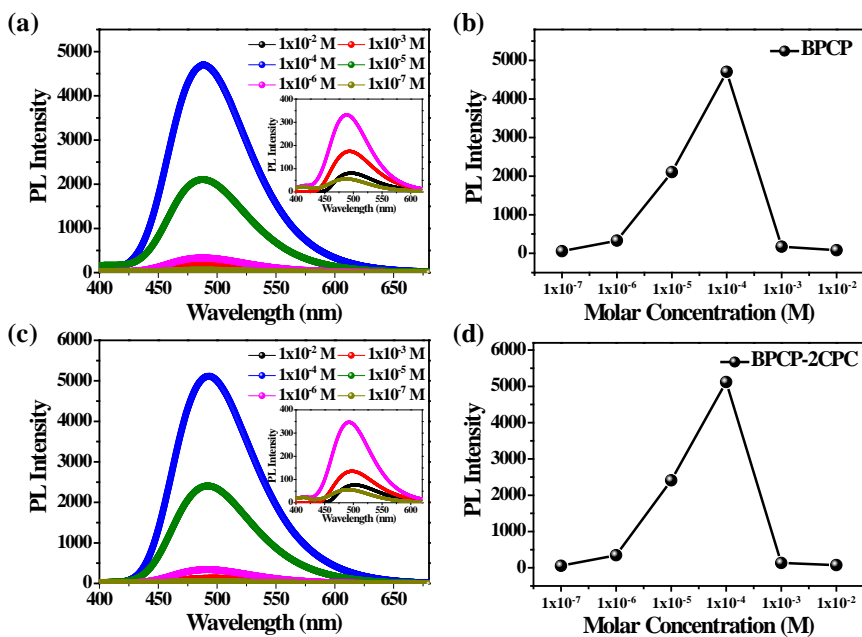


Fig. S3. PL spectra of (a) BPCP and (c) BPCP-2CPC in toluene with different molar concentration values of 10^{-2} , 10^{-3} , 10^{-4} , 10^{-5} , 10^{-6} , and 10^{-7} M. Inset shows PL spectra showing PL intensities below 1000. The plots of PL intensity versus molar concentration of (b) BPCP and (d) BPCP-2CPC.

Both materials show an increase in PL intensity up to 10^{-4} M, but after that, the PL intensity sharply decrease due to concentration quenching. This phenomenon is due to the aggregation caused quenching effect caused by shortening the distance between dopants in OLEDs.

3-3. Transient PL decay spectra of BPCP and BPCP-2CPC

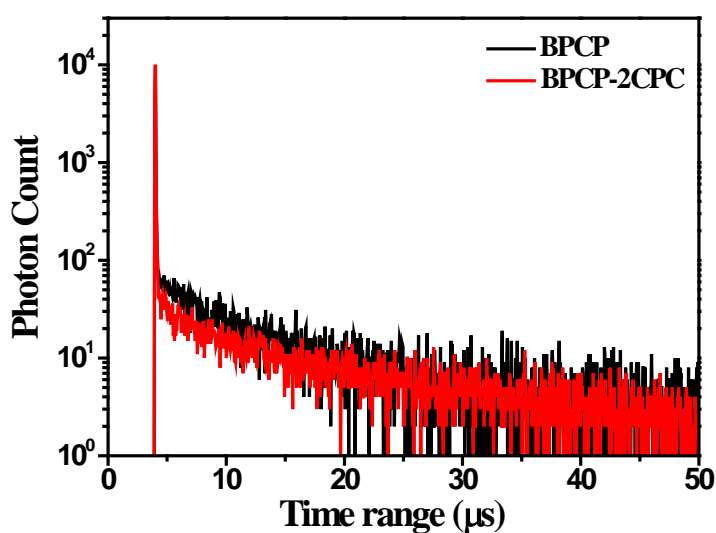


Fig. S4 Transient PL decay curves of **BPCP** and **BPCP-2CPC** films at room temperature.

Table S1 Prompt and delayed emission lifetimes of **BPCP** and **BPCP-2CPC** films from 100 to 300 K

Temperature (K)	BPCP		BPCP-2CPC	
	τ_p (ns)	τ_d (μ s)	τ_p (ns)	τ_d (μ s)
100	17.3	7.52	15.9	9.27
200	19.8	6.86	24.2	7.82
300	24.2	6.06	25.2	6.92

* τ_p and τ_d : Prompt and delayed emission lifetime, respectively.

3-4. Prompt and delayed emission spectra of BPCP and BPCP-2CPC

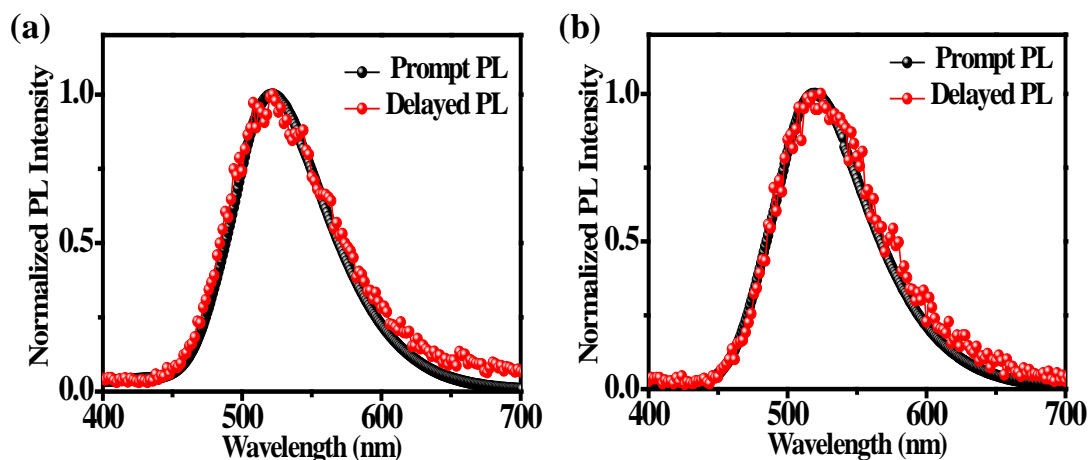


Fig. S5 Prompt and delayed emission spectra of **BPCP** and **BPCP-2CPC** films measured at room temperature.

3-5. Rate constants of BPCP and BPCP-2CPC

Table S2 Quantum efficiencies, lifetimes, and rate constants of **BPCP** and **BPCP-2CPC**

Compounds	Φ_{PL}	Φ_{p}^b	Φ_{d}^b	τ_{p}^b (ns)	τ_{d}^b (μs)	k_{p}^b (10^7 s^{-1})	k_{d}^b (10^5 s^{-1})	$k_{\text{r}}^{\text{S},b}$ (10^7 s^{-1})	k_{ISC}^b (10^7 s^{-1})	k_{RISC}^b (10^5 s^{-1})	$k_{\text{nr}}^{\text{T},b}$ (10^4 s^{-1})
BCPC	0.26 ^a / 0.60 ^b	0.43	0.17	24.2	6.06	4.13	1.65	1.78	2.35	1.16	11.5
BCPC-2CPC	0.36 ^a / 0.89 ^b	0.64	0.25	25.2	6.92	3.97	1.44	2.54	1.43	1.56	4.40

^aToluene solution under ambient conditions. ^bIn film state under nitrogen. * Φ_{PL} : Overall absolute photoluminescence quantum yield using an integrating sphere. Φ_{p} and Φ_{d} : PLQYs of the prompt (p) and delayed (d) emission estimated according to the corresponding proportions in transient decay curve, respectively. τ_{p} and τ_{d} : Prompt and delayed emission lifetimes; k_{p} and k_{d} : prompt and delayed fluorescence decay lifetime, respectively. k_{r}^{S} : Radiative decay rate constant of the singlet excited state, k_{ISC} : Rate constant for intersystem crossing (ISC) from the singlet excited state to the triplet excited state, k_{RISC} : Rate constant for reverse intersystem crossing (RISC) from the triplet excited state to the singlet excited state and k_{nr}^{T} : non-radiative (nr) decay rate constant of the triplet excited state.

The kinetic parameters of **BCPC** and **BCPC-2CPC** in the film state were determined from the experimental data (**Table S3**). The prompt (Φ_{p}) and delayed (Φ_{d}) fluorescence quantum yields were obtained from the ratio of the area under the emission peak in the transient PL spectra based on the total photoluminescence quantum yield (Φ_{PL}). The prompt (τ_{p}) and delayed (τ_{d}) fluorescence lifetimes were determined by fitting the transient PL curve. From these values, the prompt (k_{p}) and delayed (k_{d}) fluorescence decay rate constants were determined (where $k_{\text{p}} = 1/\tau_{\text{p}}$ and $k_{\text{d}} = 1/\tau_{\text{d}}$). The rate constants for radiative decay of the singlet excited state (k_{r}^{S}), intersystem crossing (k_{ISC} , $\text{S}_1 \rightarrow \text{T}_1$), and reverse intersystem crossing (k_{RISC} , $\text{T}_1 \rightarrow \text{S}_1$) were calculated using the following equations:

$$k_r^S = k_p \cdot \Phi_p \quad (1)$$

$$k_{ISC} = k_p \cdot (1 - \Phi_p) \quad (2)$$

$$k_{RISC} = (k_p \cdot k_d / k_{ISC}) \cdot (\Phi_d / \Phi_p) \quad (3)$$

$$k_{nr}^T = k_d - k_{RISC} \cdot \Phi_p \quad (4)$$

The non-radiative (nr) decay rate constant of the triplet excited state (k_{nr}^T) was obtained from Eqs. (1)–(3). The calculation is based on the assumption that the non-radiative decay rate constant of the singlet excited state (k_{nr}^S) is zero at 300 K.⁵⁻⁶

3-6. Cyclic Voltammograms

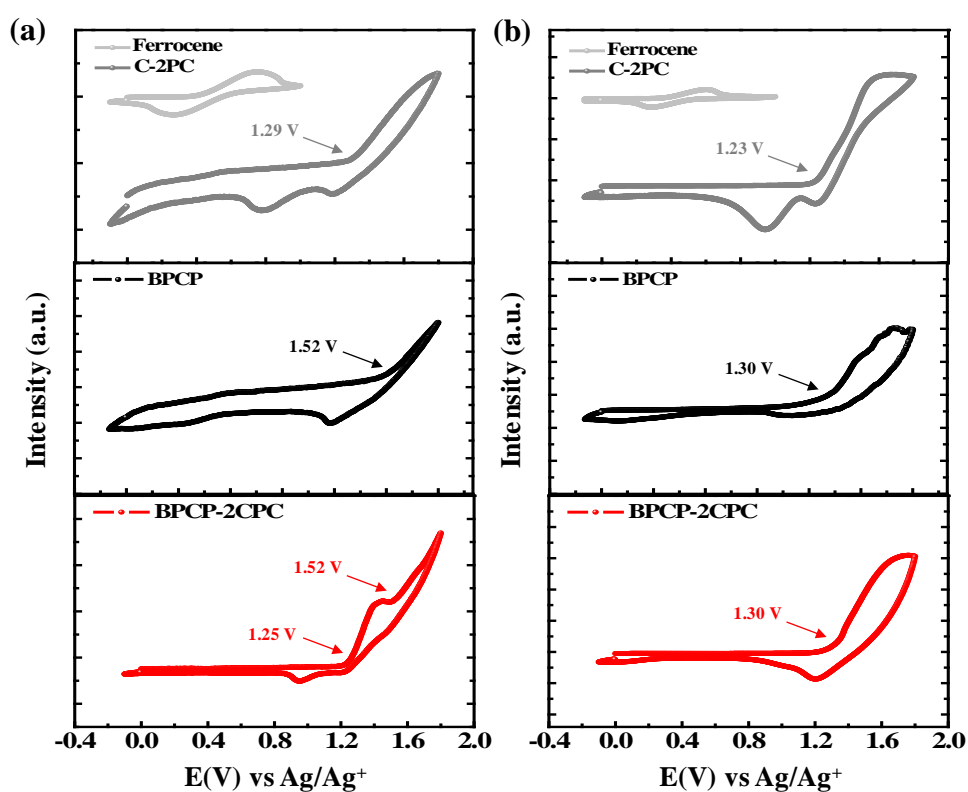


Fig. S6 Cyclic voltammograms of C-2PC, BPCP, and BPCP-2CPC in (a) solution and (b) film state.

Cyclic voltammetry (CV) analysis of the two compounds was performed in the film state to determine the HOMO and LUMO energy levels (Fig. S6b and Table 1). However, only one oxidation peak was observed for **BPCP-2CPC**, demonstrating that the oxidation potential of the donor-carbazole of the host moiety and donor-carbazole of the emissive core (**BPCP**) overlapped. In order to demonstrate the presence of the host moiety of **BPCP-2CPC**, CV experiments were carried out in dilute solutions (Fig. S6a), where both peaks were clearly identified. **C-2PC** (see Fig. S8a) is the host material in which only two phenyl-carbazole-containing molecules are linked through sp^3 -hybridized carbons in the cyclohexane unit; the detailed properties are summarized in Fig. S8 and Table S3.^{7,8}

3-7. TGA and DSC Curves

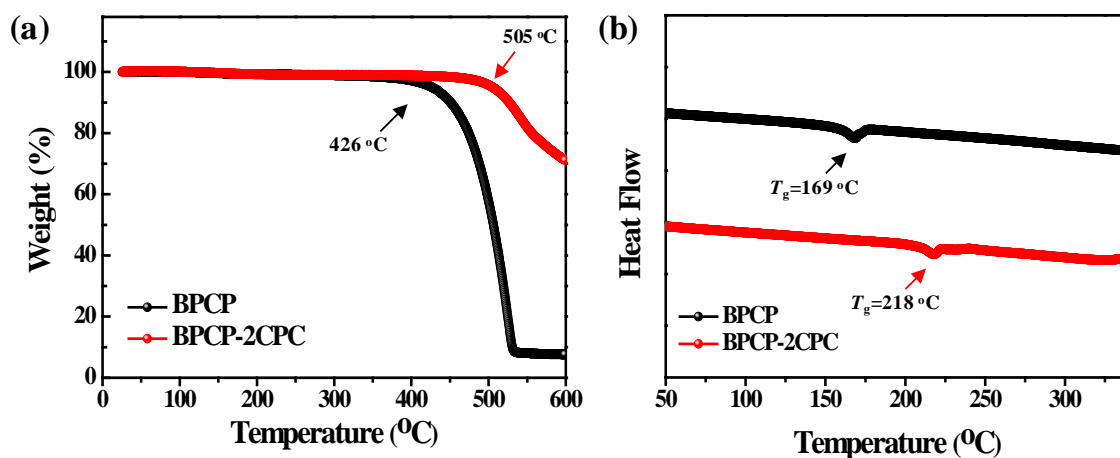


Fig. S7 (a) TGA and (b) DSC curves for **BPCP** and **BPCP-2CPC**.

The thermal properties were further evaluated using differential scanning calorimetry (DSC) and thermogravimetric analysis (TGA) under nitrogen atmosphere. **BPCP** and **BPCP-2CPC** exhibited high decomposition temperatures (T_d) of 426 and 505 °C, respectively. The glass transition temperatures (T_g) of **BPCP** and **BPCP-2CPC** were 169 and 218 °C, indicative of good thermal stability for application in OLED devices.

3-8. Photophysical and Thermal Properties of C-2PC

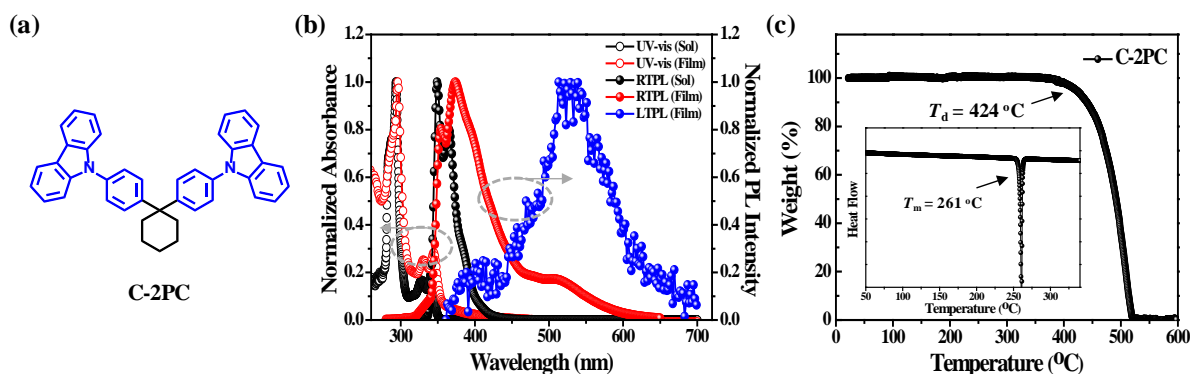


Fig. S8 (a) Chemical structure, (b) UV-vis absorption, PL spectra, and low-temperature PL, and (c) DSC/TGA curves of **C-2PC**.

Table S3 Optical, photophysical, and thermal properties of **C-2PC**

Compounds	$\lambda_{\text{max}}^{\text{abs}}$ (nm)		$\lambda_{\text{max}}^{\text{em}}^{\text{sol}}$ (nm)		$E_{\text{S}}/E_{\text{T}}/\Delta E_{\text{ST}}$ (eV) ^b	$E_{\text{g}}^{\text{opt}}$ (eV) ^c	$T_{\text{d}}/T_{\text{m}}/T_{\text{g}}$ (°C) ^d
	Sol. ^a	Film	Sol. ^a	Film			
C-2PC	293, 328, 341	296, 330, 344	349, 365	354, 374	3.669/3.062/0.607	3.48	424/261/-

^aToluene solution, ^bmeasured in the film state, ^ccalculated from the absorption threshold (film state), ^d T_{d} : decomposition temperature, corresponding to 5 wt% loss, T_{m} : melting temperature, and T_{g} : glass transition temperature.

3-9. PL spectrum of the doped film of C-2PC:BPCP

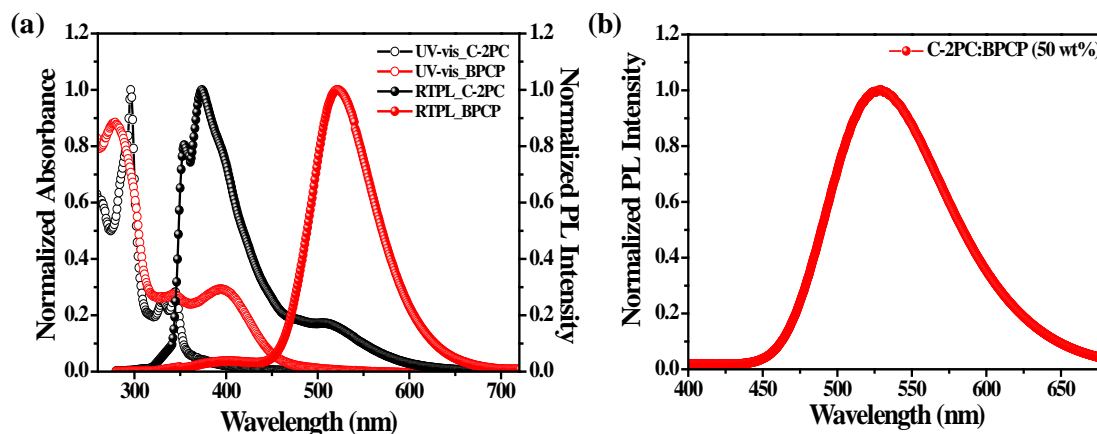


Fig. S9 (a) UV-vis absorption and PL spectra of **C-2PC** and **BPCP**, and (b) PL spectrum of the doped film of **BPCP** in **C-2PC**.

4. Fabrication and Characterization of TADF-OLED Device

The TADF-OLEDs were fabricated with the conventional device configuration: ITO/poly(3,4-ethylenedioxythiophene):poly(styrene sulfonate) (PEDOT:PSS) (40 nm)/poly(9-vinylcarbazole) (PVK) (20 nm)/EML /1,3,5-tris(1-phenyl-1H-benzimidazol-2-yl)benzene (TPBi) (40 nm)/LiF (1 nm)/Al (100 nm). Glass substrates coated with 150 nm thick indium tin oxide (ITO) with a sheet resistance of $10.0 \Omega \text{ cm}^{-2}$ (AMG Corp.) were used as the anode for the fabricated OLED devices. The surface of the ITO electrode was washed sequentially with acetone, deionized water, and isopropyl alcohol and then treated with UV-ozone for 20 min. A layer of PEDOT:PSS film as a hole-injection layer, with a thickness of 40 nm, was coated onto ITO glass (spin coating at 4000 rpm for 30 s followed by baking at 155 °C for 15 min in air). The PVK films as a hole-transporting layer were prepared from a chlorobenzene (CB) solution (0.5 wt%) and spin-coated onto the PEDOT:PSS film at 3000 rpm for 30 s. The emitting layer was then spin-coated on top of the PVK-treated substrate. Subsequently, a TPBi layer was vacuum-deposited on the previous layer as the electron transport layer. Thereafter, LiF as the electron-injection layer and Al cathode layers as the cathode were vacuum-deposited on the TPBi layer at thicknesses of about 1 nm and 100 nm, respectively. The fabricated hybrid-type devices were characterized using a Keithley SMU 236 instrument and a SpectraScan PR-655 colorimeter to evaluate the current-voltage-luminance characteristics, current, power, external quantum efficiencies, and the electroluminescence spectra of the solution-processed TADF-OLEDs.

4-1. EL Performance Data for Solution-processed Non-doped TADF-OLEDs

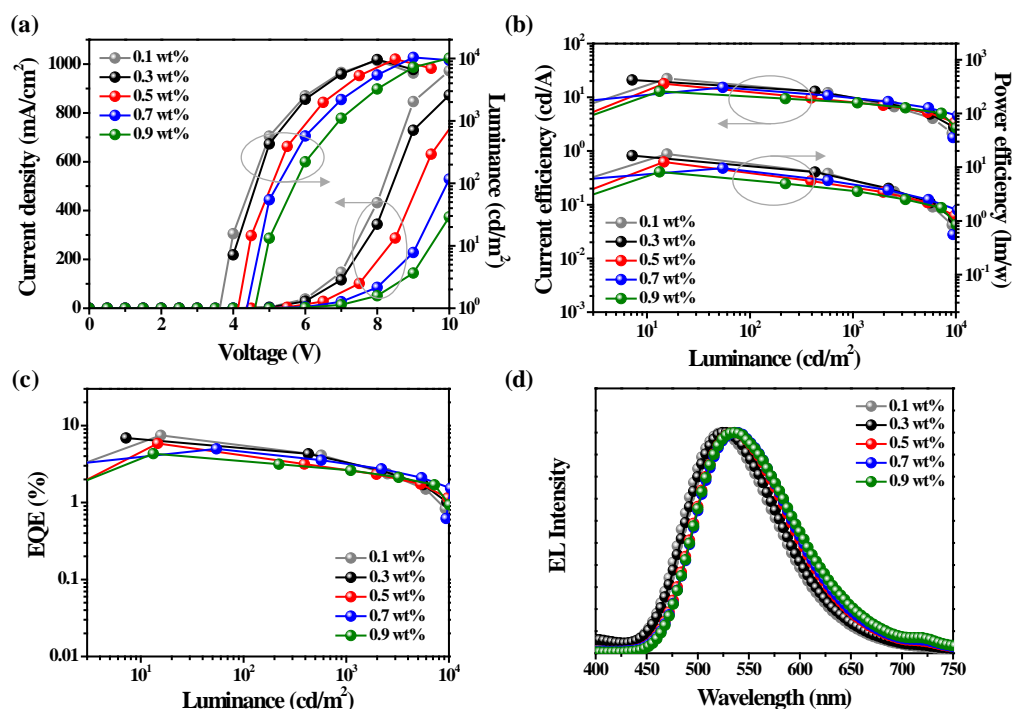


Fig. S10 (a) Current density-voltage-luminance curves, (b) current efficiency-luminance-power efficiency curves, (c) external quantum efficiency (EQE)-luminance curves, and (d) electroluminescence (EL) spectra at a luminance of 1000 cd m⁻² for solution-processed TADF-OLED devices with **BPCP** as the EML.

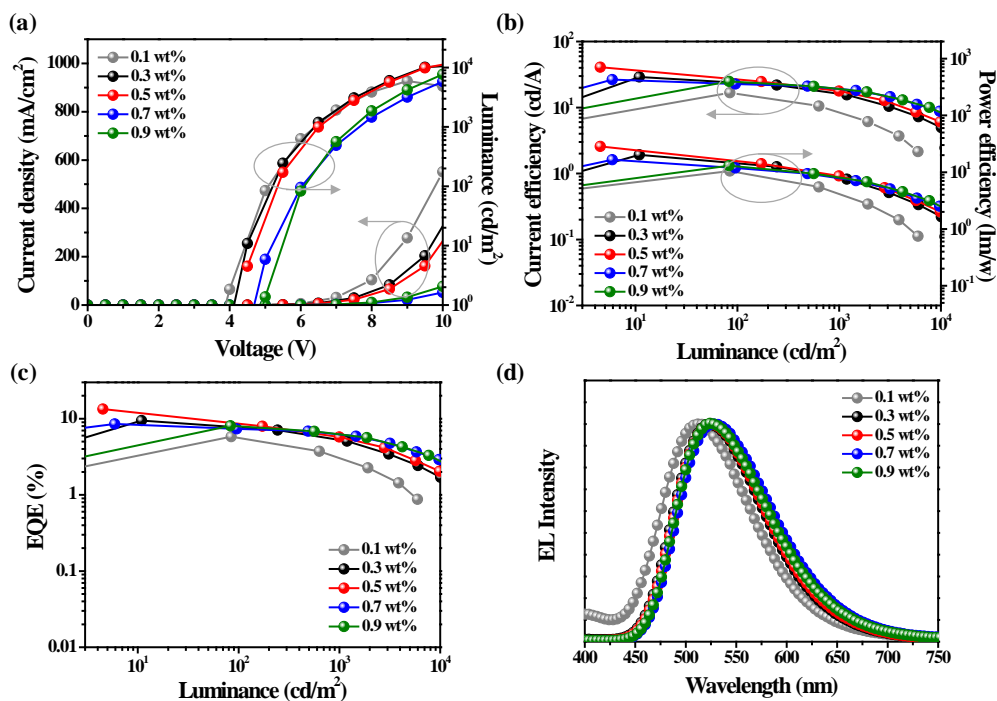


Fig. S11 (a) Current density-voltage-luminance curves, (b) current efficiency-luminance-power efficiency curves, (c) external quantum efficiency (EQE)-luminance curves, and (d) electroluminescence (EL) spectra at a luminance of 1000 cd m⁻² for solution-processed TADF-OLED devices with **BPCP-2CPC** as the EML.

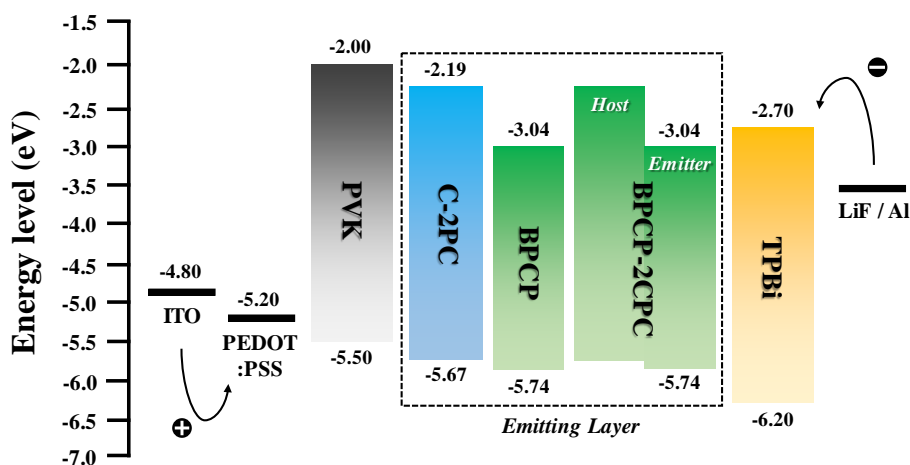
Table S4 Performance data for solution-processed TADF-OLEDs based on **BPCP** and **BPCP-2CPC**

Emitting Layer	Solution Conc. (wt%)	V_{on}^a (V)	$\eta_{c,max}^b$ (cd/A)	$\eta_{p,max}^c$ (lm/W)	L^d (cd/m ²)	η_{ext}^e (%)			λ_{EL}^f (nm)	CIE ^g (x, y)
						Max.	At 100 cd m ⁻²	At 500 cd m ⁻²		
BPCP	0.1	3.61	22.3	17.5	9245	7.46	5.52	4.36	524	(0.31, 0.52)
	0.3	3.77	21.0	16.5	9573	6.88	5.08	4.10	528	(0.32, 0.52)
	0.5	4.12	17.9	12.5	9753	5.86	4.12	3.13	536	(0.36, 0.54)
	0.7	4.37	15.2	9.55	10400	4.99	4.60	3.63	536	(0.37, 0.54)
	0.9	4.60	12.9	8.13	10090	4.31	3.43	2.94	536	(0.37, 0.54)
BPCP-2CPC	0.1	3.60	16.7	10.5	5951	5.81	5.60	3.97	512	(0.27, 0.47)
	0.3	3.65	29.0	20.3	10990	9.44	7.73	6.05	524	(0.32, 0.54)
	0.5	4.20	40.8	28.5	12780	13.4	8.70	7.04	524	(0.33, 0.54)
	0.7	4.66	26.4	16.6	14590	8.54	7.55	6.83	528	(0.34, 0.55)
	0.9	4.87	24.9	13.0	13480	8.08	7.78	6.86	528	(0.34, 0.55)

^aTurn-on voltage at 5 cd m⁻². ^bMaximum current efficiency. ^cMaximum power efficiency. ^dMaximum luminance. ^eMaximum external quantum efficiency. ^fEL peak wavelength. ^gCommission Internationale de L'Eclairage coordinates at 1000 cd m⁻². Device configuration: ITO/PEDOT:PSS (40 nm)/PVK (20 nm)/EML/TPBi (40 nm)/LiF (1 nm)/Al (100 nm).

4-2. Photophysical Properties and Device Performance for Doped TADF-OLEDs

4-2-1. Schematic Energy Level Diagrams of Doped TADF-OLED

**Figure. S12** Schematic energy level diagrams of doped system for solution-processed TADF-OLED devices employing **C-2PC**, **BPCP**, and **BPCP-2CPC**.

4-2-2. Transient PL decay spectra of C-2PC:BPCP and C-2PC:BPCP-2CPC

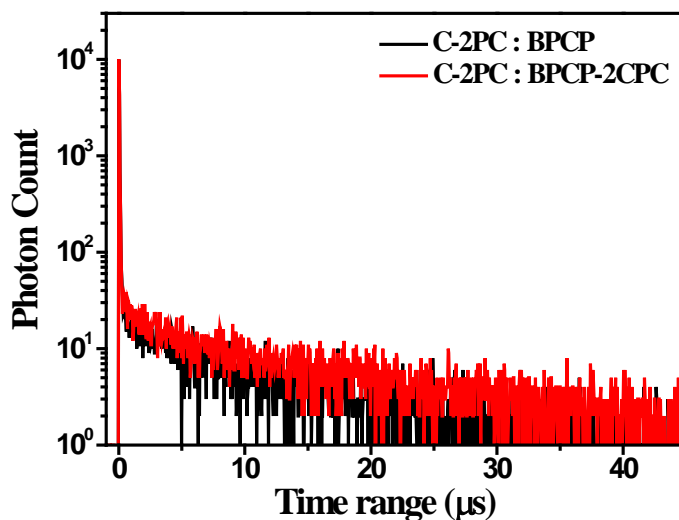


Figure. S13 Transient PL decay curves of **C-2PC:BPCP** and **C-2PC:BPCP-2CPC** films at room temperature.

4-2-3. Rate constants of C-2PC:BPCP and C-2PC:BPCP-2CPC

Table S5 Quantum efficiencies, lifetimes, and rate constants of **C-2PC:BPCP** and **C-2PC:BPCP-2CPC**. (Doping concentration = 50 wt%)

Compounds	Φ_{PL}	Φ_p^a	Φ_d^a	τ_p^a (ns)	τ_d^a (μ s)	k_p^a (10^7 s $^{-1}$)	k_d^a (10^5 s $^{-1}$)	k_r^S, a (10^7 s $^{-1}$)	k_{ISC}^a (10^7 s $^{-1}$)	k_{RISC}^a (10^5 s $^{-1}$)	k_{nr}^T, a (10^4 s $^{-1}$)
C-2PC:BCPC	0.82 ^a	0.67	0.15	27.5	4.12	3.64	2.43	2.44	1.20	1.65	13.2
C-2PC:BCPC-2CPC	0.79 ^a	0.58	0.21	26.7	6.08	3.75	1.64	2.18	1.58	1.41	8.20

^aIn film states under nitrogen. * Φ_{PL} : Overall absolute photoluminescence quantum yield using an integrating sphere, Φ_p and Φ_d : PLQYs of the prompt (p) and delayed (d) emission estimated according to the corresponding proportions in transient decay curve, τ_p and τ_d : prompt and delayed emission lifetimes, k_p and k_d : prompt and delayed fluorescence decay lifetime, respectively. k_r^S : Radiative decay rate constant of the singlet excited state, k_{ISC} : rate constant for intersystem crossing (ISC) from the singlet excited state to the triplet excited state, k_{RISC} : rate constant for reverse intersystem crossing (RISC) from the triplet excited state to the singlet excited state and k_{nr}^T : non-radiative (nr) decay rate constant of the triplet excited state.

The kinetic parameters of **C-2PC:BCPC** and **C-2PC:BCPC-2CPC** in the film state were determined from the experimental data (**Table S5**); the detailed calculation process is summarized in Section 3-5.

4-2-4. Device Performance of Solution-processed Doped TADF-OLEDs

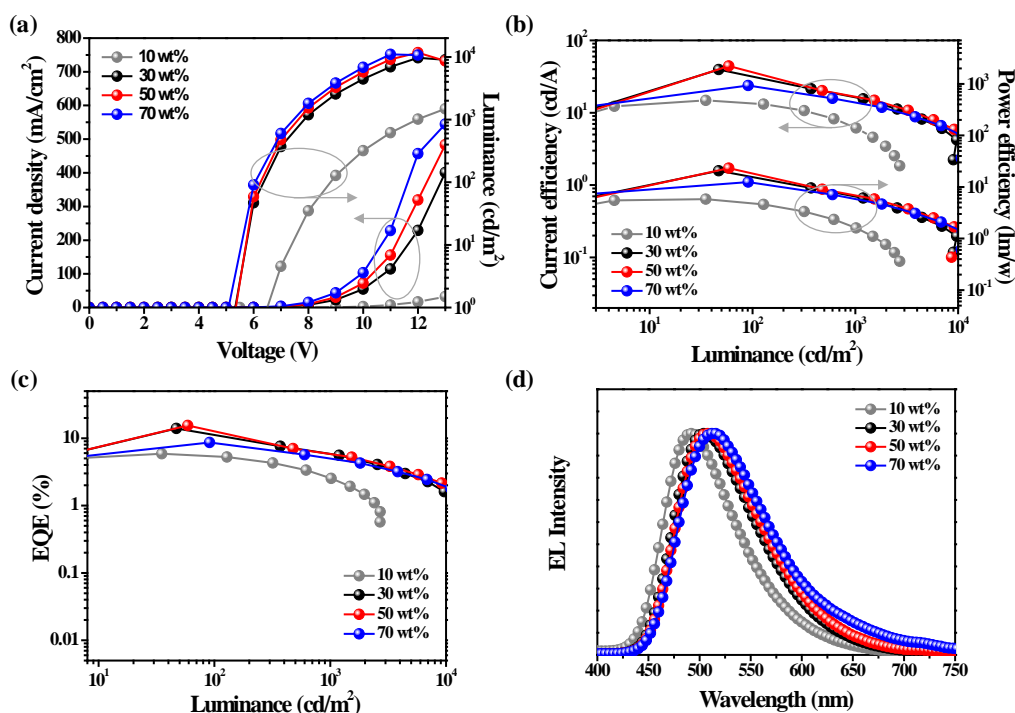


Fig. S14 (a) Current density-voltage-luminance curves, (b) current efficiency-luminance-power efficiency curves, (c) external quantum efficiency (EQE)-luminance curves, and (d) electroluminescence (EL) spectra at a luminance of 1000 cd m⁻² for solution-processed TADF-OLED devices with C-2PC:BPCP as the EML.

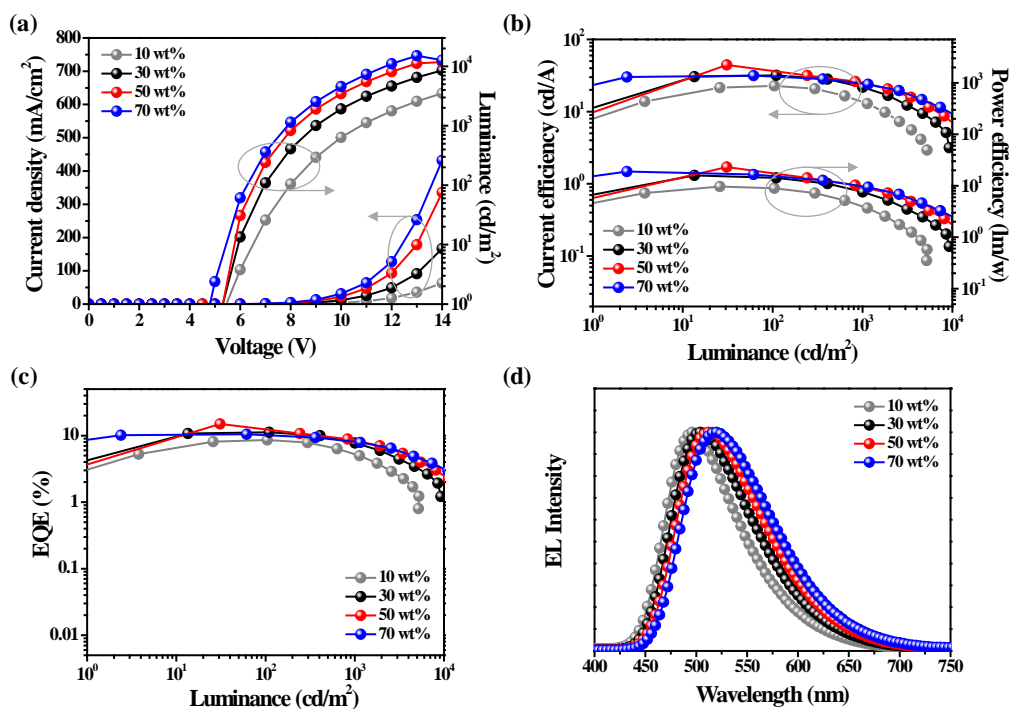


Fig. S15 (a) Current density-voltage-luminance curves, (b) current efficiency-luminance-power efficiency curves, (c) external quantum efficiency (EQE)-luminance curves, and (d) electroluminescence (EL) spectra at a luminance of 1000 cd m⁻² for solution-processed TADF-OLED devices with C-2PC:BPCP-2CPC as the EML.

Table S6 Performance data for solution-processed TADF-OLEDs based on **C-2PC:BPCP** and **C-2PC:BPCP-2CPC**

Emitting Layer	Emitter Conc. (wt%)	V_{on}^a (V)	$\eta_{c,max}^b$ (cd/A)	$\eta_{p,max}^c$ (lm/W)	L^d (cd/m ²)	η_{ext}^e (%)			λ_{EL}^f (nm)	CIE ^g (x, y)
						Max.	At 100 cd m ⁻²	At 500 cd m ⁻²		
C-2PC :BPCP	10	6.20	14.8	5.81	2701	5.87	5.41	3.71	492	(0.21, 0.40)
	30	5.01	39.5	20.7	9683	14.0	11.2	6.46	504	(0.26, 0.49)
	50	5.01	44.3	23.2	11760	15.4	12.8	6.92	508	(0.27, 0.50)
	70	5.00	23.8	12.5	11000	8.62	8.45	6.02	512	(0.30, 0.51)
C-2PC :BPCP -2CPC	10	5.20	22.7	9.62	5242	8.61	8.57	6.87	496	(0.23, 0.45)
	30	5.03	31.8	15.9	9256	11.2	11.3	9.39	504	(0.27, 0.49)
	50	5.03	44.2	23.2	11850	15.0	12.5	9.71	512	(0.29, 0.52)
	70	4.40	31.6	18.9	15090	10.4	10.1	9.07	520	(0.32, 0.54)

^aTurn-on voltage at 5 cd m⁻². ^bMaximum current efficiency. ^cMaximum power efficiency. ^dMaximum luminance. ^eMaximum external quantum efficiency. ^fEL peak wavelength. ^gCommission Internationale de L'Eclairage coordinates at 1000 cd m⁻². Device configuration: ITO/PEDOT:PSS (40 nm)/PVK (20 nm)/EML/TPBi (40 nm)/LiF (1 nm)/Al (100 nm).

We evaluated the doped OLEDs by employing **BPCP** and **BPCP-2CPC** as emitters into **C-2PC** host material having a high triplet energy ($T_I=3.062$ eV; Fig. S12). The transient PL characteristics and photophysical parameters of the doped films are shown in Fig. S13 and Table S5. The maximum EQE of the devices employing **C-2PC:BPCP** and **C-2PC:BPCP-2CPC** was obtained with doping concentrations of 50 wt% **BPCP** and **BPCP-2CPC**; the maximum EQEs of both devices was similar (15.4 and 15.0%, respectively; Fig. S14–15 and Table S6).

5. Additional Information

5-1. Surface Topology Analysis (Doped and Non-doped EML)

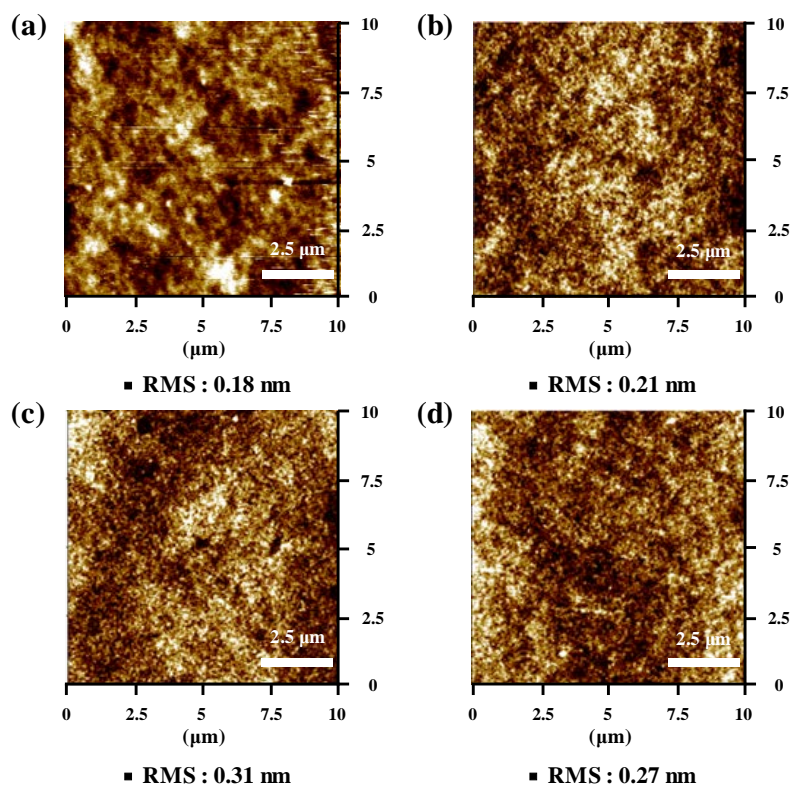


Fig. S16 AFM topographic images (10 $\mu\text{m} \times 10 \mu\text{m}$) of (a) BPCP, (b) BPCP-2CPC, (c) C-2PC:BPCP, and (d) C-2PC:BPCP-2CPC films.

6. Notes and references

- 1 K. Watanabe, D. Kumaki, T. Tsuzuki, E. Tokunaga and S. Tokito, *J. Photopolym. Sci. Technol.*, 2007, **20**, 39.
- 2 T. Oshiyama, N. Yasukawa, H. Kita, T. Matsui, M. Sumita and K. Morihashi, *Bull. Chem. Soc. Jpn.*, 2017, **90**, 195.
- 3 S. Gan, S. Hu, X. L. Li, J. Zeng, D. Zhang, T. Huang, W. Luo, Z. Zhao, L. Duan, S. J. Su and B. Z. Tang, *ACS Appl. Mater. Interfaces*, 2018, **10**, 17327.
- 4 I. S. Park, H. Seo, H. Tachibana, J. U. Kim, J. Zhang, S. M. Son and T. Yasuda, *ACS Appl. Mater. Interfaces*, 2017, **9**, 2693.
- 5 S. Y. Lee, T. Yasuda, H. Komitama, J. Lee and C. Adachi, *Adv. Mater.*, 2016, **28**, 4019.
- 6 J. S. Kang, T. R. Hong, H. J. Kim, Y. H. Son, R. Lampande, B. Y. Kang, C. Lee, J. K. Bin, B. S. Lee, J. H. Yang, J. W. Kim, S. Park, M. J. Cho and D. H. Choi, *J. Mater. Chem. C*, 2016, **4**, 4512.
- 7 T. Oshiyama, N. Yasukawa, H. Kita, T. Matsui, M. Sumita and K. Morihashi, *Bull. Chem. Soc. Jpn.*, 2017, **90**, 195.
- 8 K. Watanabe, D. Kumaki, T. Tsuzuki, E. Tokunaga and S. Tokito, *J. Photopolym. Sci. Technol.*, 2007, **20**, 39.